


Article

Stability and Electronic Properties of 1D and 2D Ca@C₆₀ Oligomers and Polymers

Yabei Wu¹, Zhonghao Zhou^{2,*} and Zhiyong Wang^{1,*} 

¹ Key Laboratory of Advanced Light Conversion Materials and Biophotonics, Department of Chemistry, Renmin University of China, Beijing 100872, China

² School of Materials Science and Engineering, Dalian Jiaotong University, Dalian 116028, China

* Correspondence: zhonghao_zhou@ruc.edu.cn (Z.Z.); zhiyongwang@ruc.edu.cn (Z.W.)

Abstract: The polymerization of fullerenes is a significant method for obtaining fullerene-based materials that possess intriguing properties. Metallofullerenes, as a notable type of fullerene derivatives, are also capable of undergoing polymerization, potentially resulting in the creation of metallofullerene polymers. However, there is currently limited knowledge regarding the polymerization process of metallofullerenes. In this study, we have selected Ca@C₆₀ as a representative compound to investigate the polymerization process of metallofullerenes. The objective of this research is to determine whether the polymerization process is energetically favorable and to examine how the electronic properties of the metallofullerene are altered throughout the polymerization process. Ca@C₆₀ is a unique metallofullerene molecule that exhibits insolubility in common fullerene solvents like toluene and carbon disulfide but is soluble in aniline. This behavior suggests a potential tendency for Ca@C₆₀ to form oligomers and polymers that resist dissolution. However, the structures and properties of polymerized Ca@C₆₀ remain unknown. We employed density functional theory calculations to investigate the stability and electronic properties of one-dimensional and two-dimensional Ca@C₆₀ oligomers and polymers. Our findings indicate that the coalescence of Ca@C₆₀ monomers is energetically favorable, with a significant contribution from van der Waals interactions between the fullerene cages. The polymerization process of Ca@C₆₀ also involves the formation of covalent linkages, including four-atom rings and C-C single bonds. The increase in the number of the Ca@C₆₀ units to three and four in the oligomer leads to a significant decrease in the HOMO-LUMO gap. In the two-dimensional polymerized Ca@C₆₀, the organization of the monomers closely resembles the spatial configuration of carbon atoms in graphene. With a direct bandgap of 0.22 eV, the polymerized Ca@C₆₀ holds potential for utilization in optoelectronic devices.

Keywords: fullerenes; metallofullerenes; density functional theory calculations



Citation: Wu, Y.; Zhou, Z.; Wang, Z. Stability and Electronic Properties of 1D and 2D Ca@C₆₀ Oligomers and Polymers. *Inorganics* **2024**, *12*, 45. <https://doi.org/10.3390/inorganics12020045>

Academic Editor: David Turner

Received: 18 December 2023

Revised: 14 January 2024

Accepted: 22 January 2024

Published: 29 January 2024



Copyright: © 2024 by the authors. Licensee MDPI, Basel, Switzerland. This article is an open access article distributed under the terms and conditions of the Creative Commons Attribution (CC BY) license (<https://creativecommons.org/licenses/by/4.0/>).

1. Introduction

Fullerenes, which typically consist of several tens of carbon atoms, are carbon allotropes with a cage-like structure. These structures possess conjugated electronic configurations and display intriguing optical, electrical and electrochemical properties [1–6]. C₆₀, the most prominent member of the fullerene family, has been extensively researched for several decades. Its derivatives have found wide-ranging applications in photovoltaic devices and have shown potential for disease treatment [7–10]. Alongside the C₆₀ monomer, there has been significant interest in studying the polymerized form of C₆₀. Reports suggest that when exposed to photo irradiation or high pressure treatment, C₆₀ molecules can polymerize into oligomers and polymers [11,12]. The properties of the C₆₀ polymers have been explored through theoretical and experimental studies [3,13–16]. During the polymerization process, the reaction between two neighboring C₆₀ molecules typically occurs via a [2 + 2] cycloaddition mechanism, leading to the formation of a cyclobutane ring that connects two fullerene cages. Subsequent to polymerization, the resulting products usually

exhibit high insolubility in solvents that can dissolve C_{60} [16]. The structural composition of the products derived from C_{60} sample is determined by the reaction conditions. The formation of polymers and metastable materials occurs when the pressure exceeds several GPa and the temperature surpasses several hundred degrees Celsius. At higher pressures and temperatures, the C_{60} cage can rupture, leading to the production of diamond-like materials [16,17]. Sabirov utilized density-functional theory to examine the polarizability of fullerene oligomers $(C_{60})_n$ ($n = 1-5$) [18]. The study findings demonstrated that the average polarizability of $(C_{60})_n$ is not linearly correlated with the number of fullerene cores in the molecules, suggesting a violation of additivity. This phenomenon, referred to as the exaltation of polarizability, arises from the interaction between the π -electronic systems of the fullerene cores in $(C_{60})_n$ and becomes increasingly significant as the distance between them increases. Quantum chemical calculations of fullerene oligomers are expensive because of the large size of the oligomers. Sabirov investigated energy, topology, and information theoretic descriptors, and obtained a ternary energy-topology-symmetry law. The findings indicate that topological indices are effective in identifying the most and least reactive atoms within the fullerene dimer structure [19].

Recently, the synthesis of monolayer and few-layer two-dimensional fullerene networks has been reported [20,21]. In the polymeric C_{60} monolayer, the C_{60} molecules are covalently bonded, showcasing excellent crystallinity and thermodynamic stability. Measurements of the electronic band structure of the polymeric C_{60} monolayer indicate a bandgap of approximately 1.6 eV. The two-dimensional crystalline polymer of C_{60} has been coined “graphullerene” and serves as a bridge between molecular and extended carbon materials. The synthesis of graphullerene involves the growth of single crystals of layered polymeric Mg_4C_{60} , followed by the removal of magnesium atoms [20,21]. Theoretical studies reveal that graphullerene is a meta-stable semiconductor with an indirect band gap [22].

Metallofullerenes, as a notable type of fullerene derivatives, may also have the ability to polymerize and form metallofullerene polymers. However, there is currently limited knowledge regarding the polymerization process of metallofullerenes. The aim of this study is to investigate the stability and electronic properties of polymerized metallofullerenes, a previously unexplored area of research. A variety of metal elements can be accommodated within the interior cavity of fullerene cages. Metallofullerene molecules have been extensively studied in terms of their synthesis, structures, and properties [23–33]. The arc-discharge technique is commonly employed for the synthesis of various metallofullerenes. While some metallofullerenes are soluble in organic solvents like toluene and carbon disulfide, others are not. One notable metallofullerene, $Ca@C_{60}$, is soluble in aniline but insoluble in toluene and carbon disulfide [34]. This can be attributed to its reactivity towards polymerization and its lack of solubility in non-polar organic solvents. The solubility in aniline may be due to the formation of a charge-transfer complex. Currently, the understanding of the structure and characteristics of polymerized $Ca@C_{60}$ is very limited. To address this gap, our study focuses on examining the stability and electronic properties of $Ca@C_{60}$ oligomers and polymers using density functional theory (DFT) calculations. We also analyze the interactions between individual $Ca@C_{60}$ monomers.

2. Results and Discussion

In a previous study by Kubozono and co-workers, endohedral metallofullerene $Ca@C_{60}$ was prepared and extracted [34]. The preparation involved arc-heating graphite rods containing CaO, followed by extraction with aniline under an air atmosphere. The laser desorption time-of-flight mass spectra of the extracted solutions showed prominent peaks attributed to $Ca@C_{60}$, demonstrating the stability of $Ca@C_{60}$. We conducted DFT calculations on $Ca@I_h-C_{60}$. Figure 1a illustrates the DFT-optimized structure of $Ca@C_{60}$. Upon encapsulation of a Ca atom, the molecule’s symmetry is reduced from I_h to C_{2v} . The Ca atom is positioned adjacent to a carbon-carbon bond, with a distance of 2.45 Å between the Ca atom and the carbon atom in the bond. In some metallofullerenes, the metal

atom resides in close proximity to the center of a six-member carbon atom ring, while the coordination occurring at a carbon-carbon bond results in an increase in energy. Regarding Ca@C_{60} , it is observed that the Ca atom is situated near a carbon-carbon bond and remains in an off-center position. If the Ca atom were to shift towards the center of the molecule, there would be a noticeable increase in the overall energy.

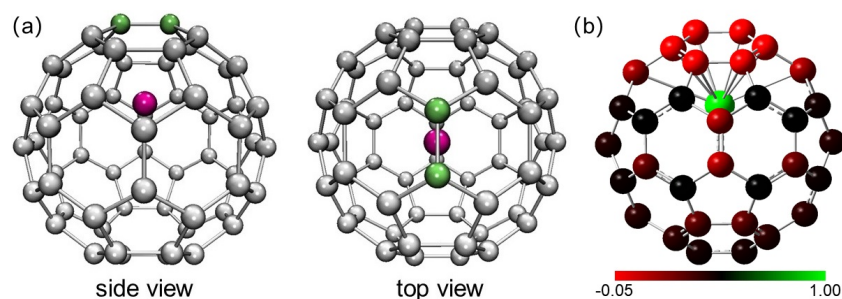


Figure 1. (a) Two views of the optimized structure of Ca@C_{60} . The carbon atoms adjacent to the Ca atom are indicated with a green color. (b) The charge distribution on the atoms of Ca@C_{60} . The green and red color indicates positive and negative charges, respectively. The black color indicates neutral atoms.

The HOMO-LUMO gap of Ca@C_{60} is calculated to be 1.14 eV. To assess the charge distribution, we conducted a natural population analysis (NPA), revealing a NPA charge of 1.8 for the Ca atom. Considering that the Ca atom possesses two valence electrons, the calculated NPA charge signifies a transfer of two electrons to the fullerene cage. Therefore, the formal charge of Ca atom can be regarded as +2. The charge distribution of Ca@C_{60} is illustrated in Figure 1b. It is evident that the negative charges on the fullerene cage are distributed unevenly. In particular, the carbon atoms in close proximity to the Ca atom exhibit a greater concentration of negative charges.

The C_{60} cage contains two types of C-C bonds. One type corresponds to the hexagon-hexagon ring junction, known as the (6,6) bond, while the other corresponds to the pentagon-hexagon ring junction, known as the (5,6) bond. In our previous research, we investigated the reactivity of the (5,6) and (6,6) bonds in Ca@C_{60} towards Diels-Alder cycloaddition reactions using density functional methods [35]. For the pristine C_{60} , the reactivity of the (6,6) bond is much higher than that of the (5,6) bond. We found that for the Diels-Alder mono-addition reaction, the unreactive (5,6) bond in C_{60} can be effectively activated by encapsulating a Ca atom. The enhancement of reactivity is attributed to both electron transfer from the metal atom to the fullerene cage and the interaction between the metal cation and the cage. The functionalization of Ca@C_{60} leads to significant increases in the HOMO-LUMO gap, which can improve the chemical stability of Ca@C_{60} . For the formation of oligomers of Ca@C_{60} , both the (5,6) and (6,6) bonds could serve as reaction sites. Consequently, various structures of Ca@C_{60} oligomers were considered in this study.

It has been reported that the metallofullerene Li@C_{60} can form dimers in solid states [36]. In the dimer of Li@C_{60} , the fullerene cages are connected by a single C-C bond. In our study on the dimer $[\text{Ca@C}_{60}]_2$, four possible isomers were considered. Isomer 1, referred to as $[\text{Ca@C}_{60}]_2$ -1, consists of two fullerene cages connected by a single C-C bond (Figure 2a). Isomers 2–4, on the other hand, involve the linkage of the fullerene cages through a four-atom ring (Figure 2b–d). Isomers 2–4 can be seen as the result of [2 + 2] cycloaddition reactions between two Ca@C_{60} molecules. Three products were considered from the [2 + 2] cycloaddition reactions between two Ca@C_{60} molecules. The product formed by connecting two (6,6) bonds is labeled as $[\text{Ca@C}_{60}]_2$ -2 (Figure 2b). The product formed by connecting two (5,6) bonds is labeled as $[\text{Ca@C}_{60}]_2$ -3 (Figure 2c). Finally, the product formed by connecting a (6,6) bond and a (5,6) bond is labeled as $[\text{Ca@C}_{60}]_2$ -4 (Figure 2d). Our DFT calculations revealed that $[\text{Ca@C}_{60}]_2$ -3 has the lowest energy, indicating that the dimerization of Ca@C_{60} prefers to occur at the (5,6) bond of the fullerene cage. This situation

is different from the C_{60} dimer. In the case of C_{60} dimer, the fullerene cages are connected by cycloaddition reaction between two (6,6) bonds. Once metal atoms are encapsulated, the cage's reactivity is altered due to electron transfer from the metal atom to the fullerene cage. As previously discussed, the unreactive (5,6) bond in C_{60} can be effectively activated by encapsulating a Ca atom in the context of the Diels-Alder mono-addition reaction. It is a common trend that the reactivity of the (5,6) bond towards Diels-Alder reactions is heightened in the case of metallofullerenes compared to empty fullerenes.

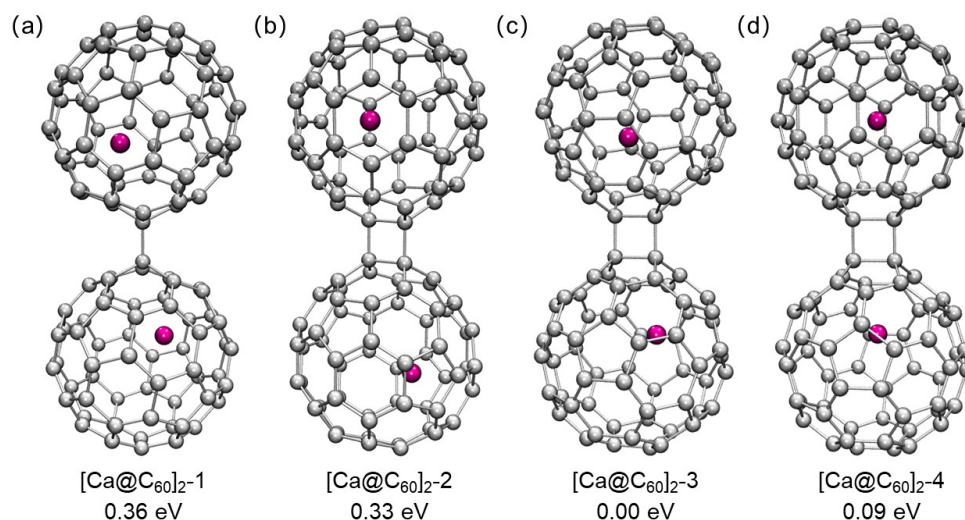


Figure 2. The optimized structures of the dimers $[Ca@C_{60}]_2$. The calculated relative energies are shown.

We examined five isomers of the trimers $[Ca@C_{60}]_3$. The first isomer, $[Ca@C_{60}]_{3-1}$, is formed by linking three $Ca@C_{60}$ molecules with C-C single bonds (Figure 3a). Isomers 2–4 can be regarded as the product of $[2 + 2]$ cycloaddition reactions between three $Ca@C_{60}$ molecules. In $[Ca@C_{60}]_{3-2}$, only (6,6) bonds are involved in the cycloaddition reactions (Figure 3b), while in $[Ca@C_{60}]_{3-3}$, only (5,6) bonds are involved (Figure 3c). In $[Ca@C_{60}]_{3-4}$, the four-atom ring connecting the fullerene cages is formed by a (6,6) bond and a (5,6) bond (Figure 3d). In $[Ca@C_{60}]_{3-5}$, the three fullerene cages are arranged in a triangular shape and connected by a four-atom ring and two C-C single bonds (Figure 3e). The four-atom ring is formed by cycloaddition reaction between two (5,6) bonds. DFT calculations indicate that $[Ca@C_{60}]_{3-5}$ has the lowest energy, making the triangular trimer more thermodynamically stable than the linear isomers.

For the tetramers $[Ca@C_{60}]_4$, we considered six isomers. Isomers 1–4, which are linear molecules (Figure 4a–d), have a bonding pattern similar to isomers 1–4 of the trimers. The fifth isomer, $[Ca@C_{60}]_{4-5}$, has a rectangular shape, with four fullerene cages connected by two four-atom rings and two single bonds (Figure 4e). In the sixth isomer, $[Ca@C_{60}]_{4-6}$, the fullerene cages form a rhombus shape (Figure 4f). DFT calculations show that $[Ca@C_{60}]_{4-5}$ and $[Ca@C_{60}]_{4-6}$ have significantly lower energy compared to the other isomers. The arrangement of the fullerene cages in $[Ca@C_{60}]_{4-6}$ is similar to the reported two-dimensional monolayer C_{60} polymer “graphullerene” [20–22]. The computed charge distribution of the atoms in $[Ca@C_{60}]_{4-5}$ and $[Ca@C_{60}]_{4-6}$ is depicted in Figure 4e,f. It is evident that the negative charges on the fullerene cage are concentrated in close proximity to the Ca atom. Consequently, there exists a robust electrostatic attraction between the negatively charged fullerene cage and the Ca cation.

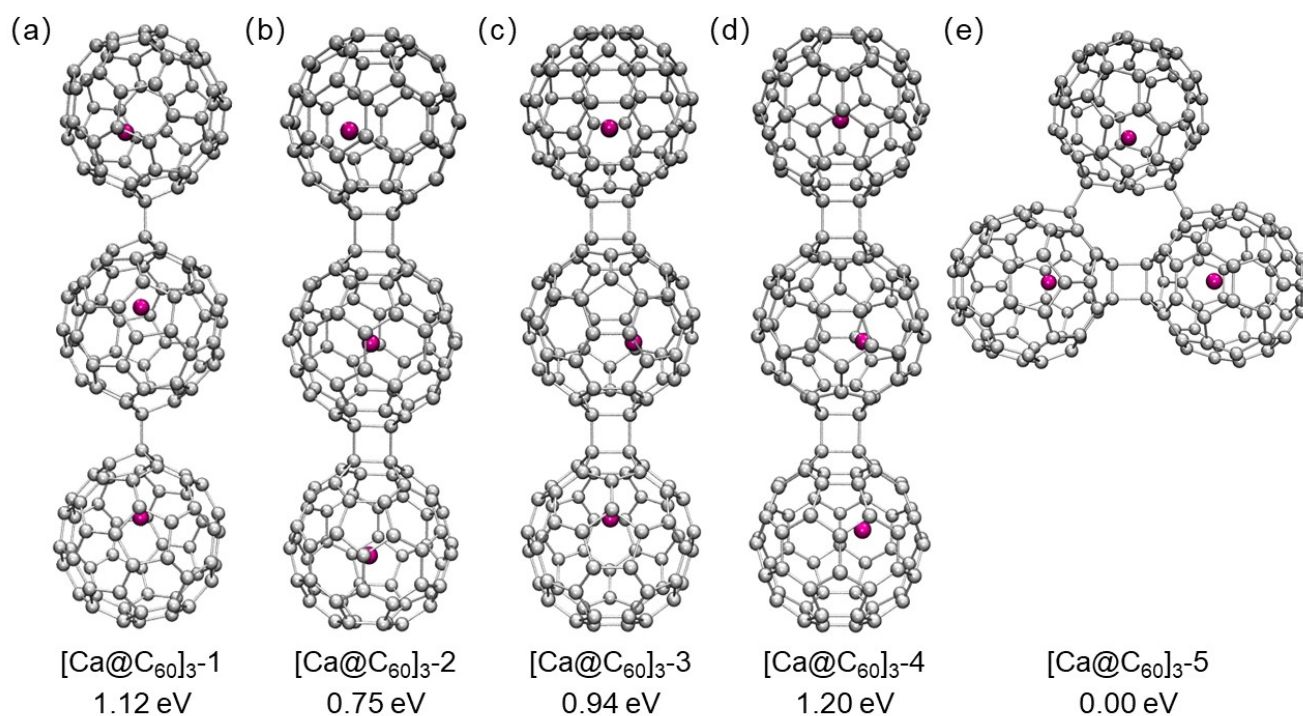


Figure 3. The optimized structures of the trimers [Ca@C₆₀]₃. The calculated relative energies are shown.

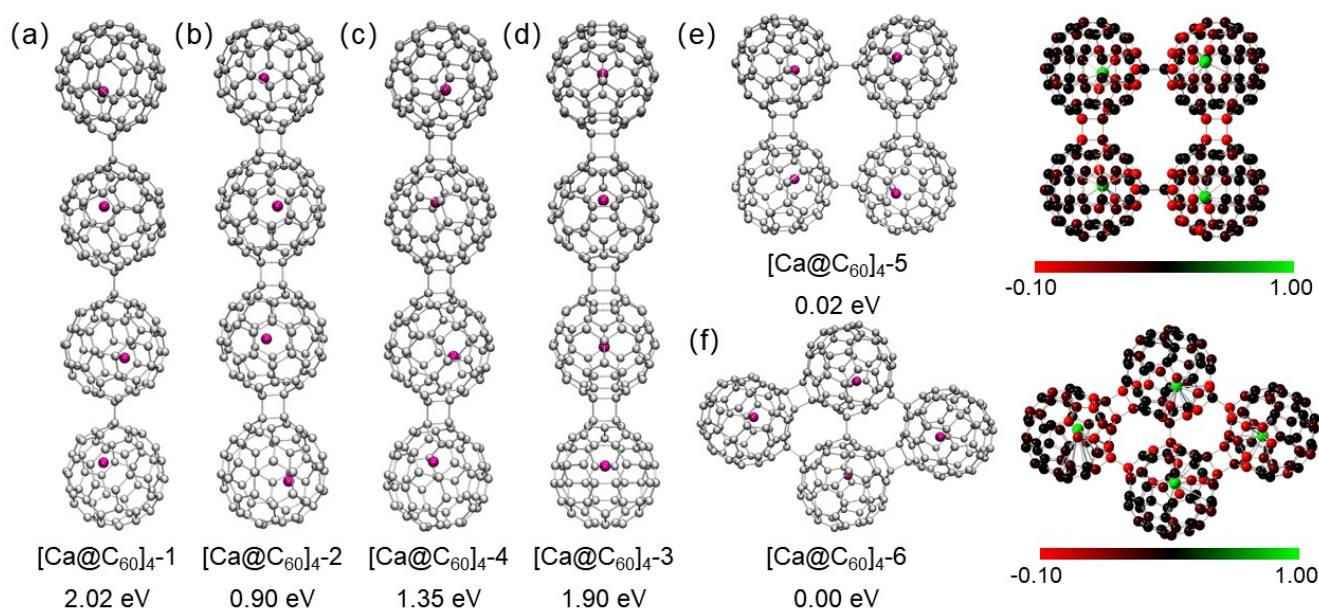


Figure 4. The optimized structures of the tetramers [Ca@C₆₀]₄. The calculated relative energies are shown.

Figure 5 depicts the molecular orbital diagrams for Ca@C₆₀, [Ca@C₆₀]₂₋₃, [Ca@C₆₀]₃₋₅ and [Ca@C₆₀]₄₋₆. DFT calculations reveal a significant alteration in the HOMO-LUMO gap of the oligomers [Ca@C₆₀]_n compared to the monomer Ca@C₆₀. The HOMO-LUMO gaps for Ca@C₆₀, [Ca@C₆₀]₂₋₃, [Ca@C₆₀]₃₋₅ and [Ca@C₆₀]₄₋₆ are 1.14, 1.36, 0.60 and 0.27 eV, respectively. The dimer [Ca@C₆₀]₂₋₃ shows an enlarged HOMO-LUMO gap in comparison to Ca@C₆₀. For the trimer and tetramers, the HOMO-LUMO gap substantially decreases as the number of Ca@C₆₀ units increases. The HOMO-LUMO gaps for other isomers of the oligomers are summarized in Table 1. In the case of empty C₆₀, the HOMOs and LUMOs

are degenerate, with the HOMOs being five-fold degenerate and the LUMOs being triply degenerate. However, when a Ca atom is encapsulated, two electrons occupy the LUMO of C_{60} , resulting in the HOMO of $Ca@C_{60}$ having a similar shape to the LUMO of C_{60} . Additionally, the LUMO and LUMO+1 of $Ca@C_{60}$, which are derived from the LUMOs of C_{60} , are almost degenerate. Similarly, the HOMO-6 to HOMO-1 of $Ca@C_{60}$, which are derived from the five-fold HOMOs of C_{60} , have very close energies.

In the case of the dimer $[Ca@C_{60}]_{2-3}$, both the HOMO and LUMO are observed to be spread across two fullerene cages. Additionally, the HOMO is also observed to be present at the C-C bridge that connects the fullerene cages. Moving on to the trimer $[Ca@C_{60}]_{3-5}$, it can be observed that the HOMO and LUMO are primarily distributed at the two fullerene cages that are connected by a four-atom ring. In the case of the tetramers $[Ca@C_{60}]_{4-6}$, the HOMO and LUMO are distributed across the two fullerene cages, which are separated by a significant distance.

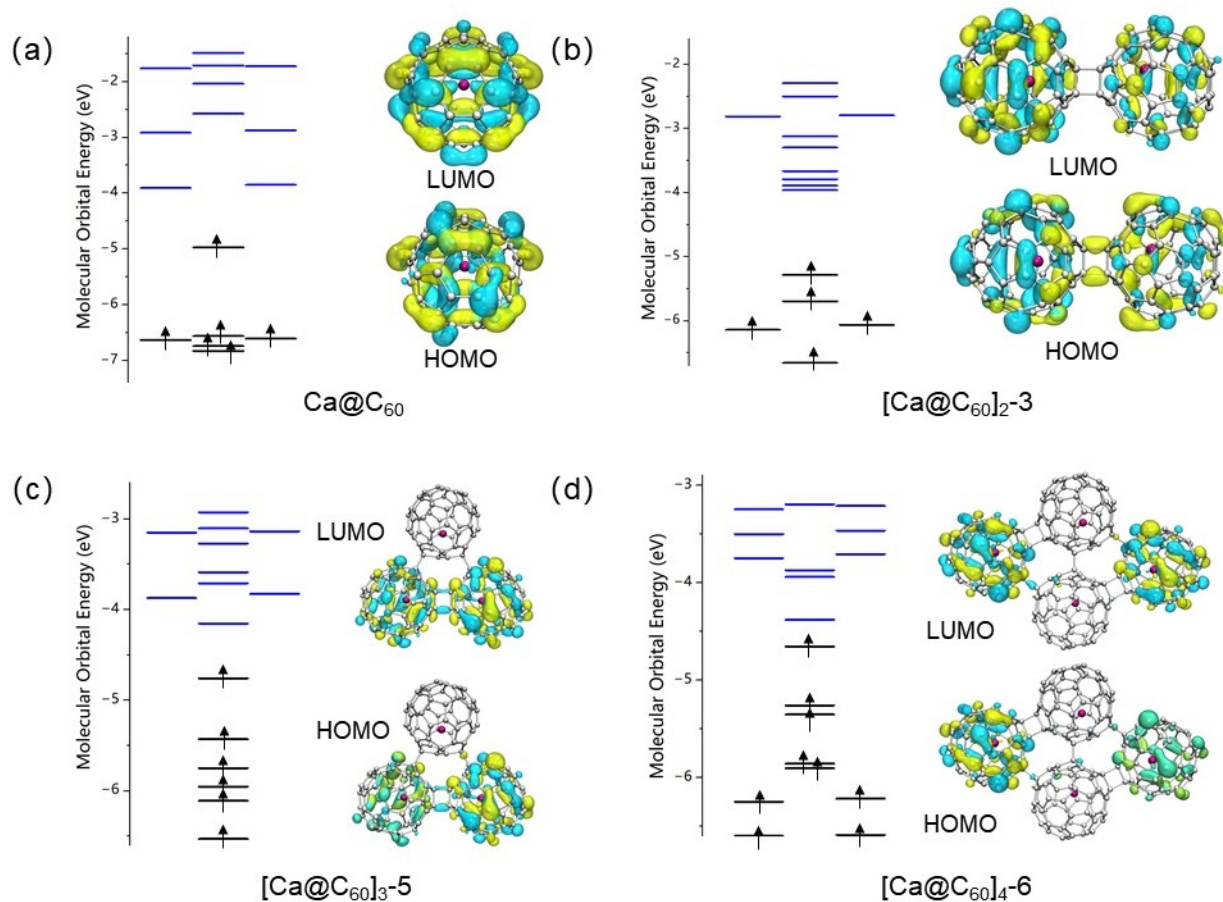


Figure 5. The calculated molecular orbital diagrams for (a) $Ca@C_{60}$, (b) $[Ca@C_{60}]_{2-3}$, (c) $[Ca@C_{60}]_{3-5}$ and (d) $[Ca@C_{60}]_{4-6}$. The occupied and unoccupied molecular orbitals are denoted in black and blue, respectively.

Table 1. The DFT-calculated HOMO-LUMO gaps (in eV) of $Ca@C_{60}$ and its oligomers.

	HOMO-LUMO Gap
$Ca@C_{60}$	1.14
2-1	0.50
2-2	1.07
2-3	1.36
2-4	0.94

Table 1. Cont.

	HOMO-LUMO Gap
3-1	0.22
3-2	1.02
3-3	1.21
3-4	0.79
3-5	0.60
4-1	0.14
4-2	1.05
4-3	1.14
4-4	0.80
4-5	0.38
4-6	0.27

The UV-vis-NIR absorption spectra for Ca@C_{60} , $[\text{Ca@C}_{60}]_{2-3}$, and $[\text{Ca@C}_{60}]_{3-5}$ are presented in Figure 6. It is observed that both Ca@C_{60} and $[\text{Ca@C}_{60}]_{2-3}$ exhibit an absorption onset at approximately 1000 nm, with a prominent absorption peak at around 800 nm. Notably, $[\text{Ca@C}_{60}]_{3-5}$ displays a broad absorption peak spanning the range of 1400–3000 nm, which can be attributed to its small HOMO-LUMO gap. This characteristic suggests potential applications in the fields of biomedicine and optoelectronic devices. On the other hand, the TDDFT calculations for $[\text{Ca@C}_{60}]_{4-6}$ were unsuccessful due to the high computational cost.

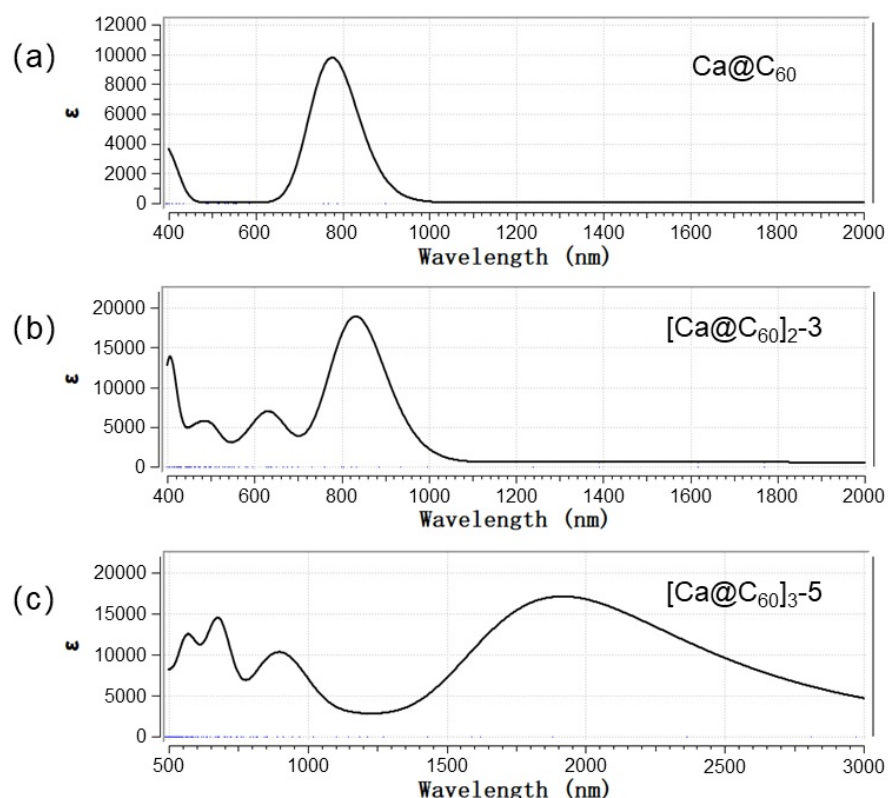


Figure 6. The calculated UV-vis-NIR absorption spectra for (a) Ca@C_{60} , (b) $[\text{Ca@C}_{60}]_{2-3}$ and (c) $[\text{Ca@C}_{60}]_{3-5}$ by using the TDDFT method.

On the basis of DFT calculations, we compared the energy between the oligomers $[\text{Ca@C}_{60}]_n$ and the monomer Ca@C_{60} . The results indicate that the formation of oligomers is an exothermic process. We calculated the relative energies for $[\text{Ca@C}_{60}]_n$ per Ca@C_{60} unit using the monomer Ca@C_{60} as a reference. The calculated values for $[\text{Ca@C}_{60}]_{2-3}$,

$[\text{Ca}@C_{60}]_{3-5}$, $[\text{Ca}@C_{60}]_{4-5}$ and $[\text{Ca}@C_{60}]_{4-6}$ per $\text{Ca}@C_{60}$ unit are -0.54 , -0.67 , -0.69 and -0.70 eV, respectively, revealing significantly lower energies compared to the monomer $\text{Ca}@C_{60}$. Remarkably, the relative energy decreases with an increase in the number of $\text{Ca}@C_{60}$ units. Consequently, the process of polymerizing $\text{Ca}@C_{60}$ exhibits a favorable energy profile.

The stability of the oligomers $[\text{Ca}@C_{60}]_n$ can be attributed to two factors. Firstly, the covalent bonding between the fullerene cages plays a crucial role. Secondly, the van der Waals interaction between the fullerene cages also contributes to the stability. To illustrate this, we examined the dimer $[\text{Ca}@C_{60}]_{2-3}$ as a representative compound and calculated the dispersion energy between the two fullerene units. This was achieved by performing energy decomposition using dispersion corrected density functional theory (DFT-D3). The calculated dispersion energy was found to be 0.49 eV, indicating that the dispersion energy significantly contributes to the dimer formation. To visualize the weak interactions between the fullerene cages, we conducted an analysis using the Independent Gradient Model based on Hirshfeld partition (IGMH) for $[\text{Ca}@C_{60}]_{2-3}$, $[\text{Ca}@C_{60}]_{3-5}$, and $[\text{Ca}@C_{60}]_{4-6}$. The results are presented in Figure 7. The isosurface of δg indicates the region where dispersion interaction is present. It is evident that dispersion interaction exists between the fullerene cages.

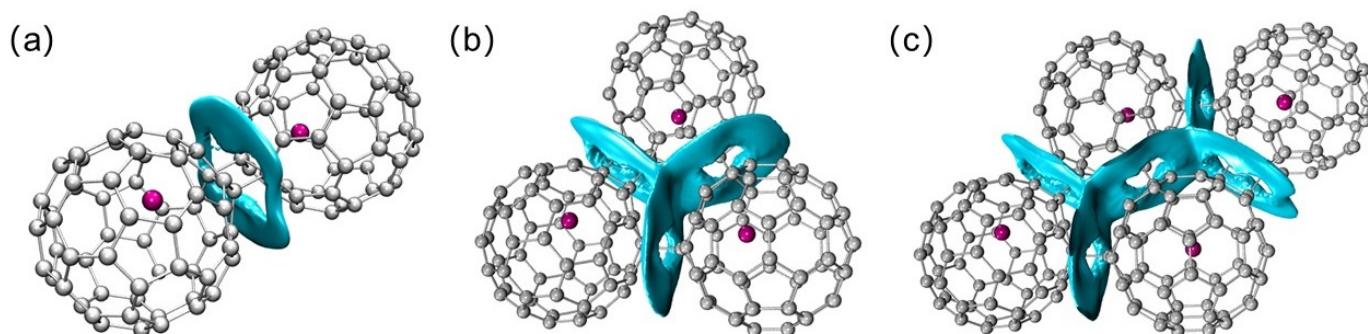


Figure 7. IGMH- δg isosurface (isovalue = 0.001 a.u.) showing the dispersion interaction between the $\text{Ca}@C_{60}$ fragments for (a) $[\text{Ca}@C_{60}]_{2-3}$, (b) $[\text{Ca}@C_{60}]_{3-5}$ and (c) $[\text{Ca}@C_{60}]_{4-6}$.

For the two-dimensional polymers $[\text{Ca}@C_{60}]_{\infty}$, we considered two possible structures. The first one, $[\text{Ca}@C_{60}]_{\infty-1}$, is constructed by extension of the $\text{Ca}@C_{60}$ units in $[\text{Ca}@C_{60}]_{4-6}$. The second one, $[\text{Ca}@C_{60}]_{\infty-2}$, is constructed by extension of the $\text{Ca}@C_{60}$ units in $[\text{Ca}@C_{60}]_{4-5}$. Figure 8 displays the optimized structures of these polymers. In $[\text{Ca}@C_{60}]_{\infty-1}$, each fullerene cage is connected to six adjacent cages, resembling a “graphullerene” structure [20–22]. In $[\text{Ca}@C_{60}]_{\infty-2}$, each fullerene cage connects with four adjacent cages. DFT calculations indicate that $[\text{Ca}@C_{60}]_{\infty-1}$ is thermodynamically more stable than $[\text{Ca}@C_{60}]_{\infty-2}$. The energy difference for the unit cell containing two $\text{Ca}@C_{60}$ units is 1.08 eV. Figure 9 shows the band structure for $[\text{Ca}@C_{60}]_{\infty-1}$, with a direct bandgap of 0.22 eV. Notably, this bandgap is significantly smaller in comparison to that of “graphullerene” [20,22]. This reduction in bandgap can be attributed to the transfer of electrons from Ca atoms to the fullerene cage. As a result, a portion of the conduction band of “graphullerene” is occupied by these transferred electrons. Consequently, the polymer $[\text{Ca}@C_{60}]_{\infty-1}$ exhibits distinct electronic characteristics in comparison to “graphullerene”. The band structure of $[\text{Ca}@C_{60}]_{\infty-1}$ reveals that the wave vectors corresponding to the Conduction band minimum (CBM) and Valance band maximum (VBM) are both situated at the high symmetry point G in the Brillouin zone. The electron transition mode displays vertical transitions, while the band structure itself demonstrates direct bandgap characteristics. Notably, since the CBM and VBM coincide at the same momentum point, the transition from the valence band to the conduction band in $[\text{Ca}@C_{60}]_{\infty-1}$, upon absorption of photons by electrons, only requires adherence to the energy conservation constraint, without necessitating additional phonon

interaction. In comparison with indirect bandgap materials, $[\text{Ca@C}_{60}]_{\infty-1}$ exhibits superior quantum efficiency, rendering it a promising contender for optoelectronic devices.

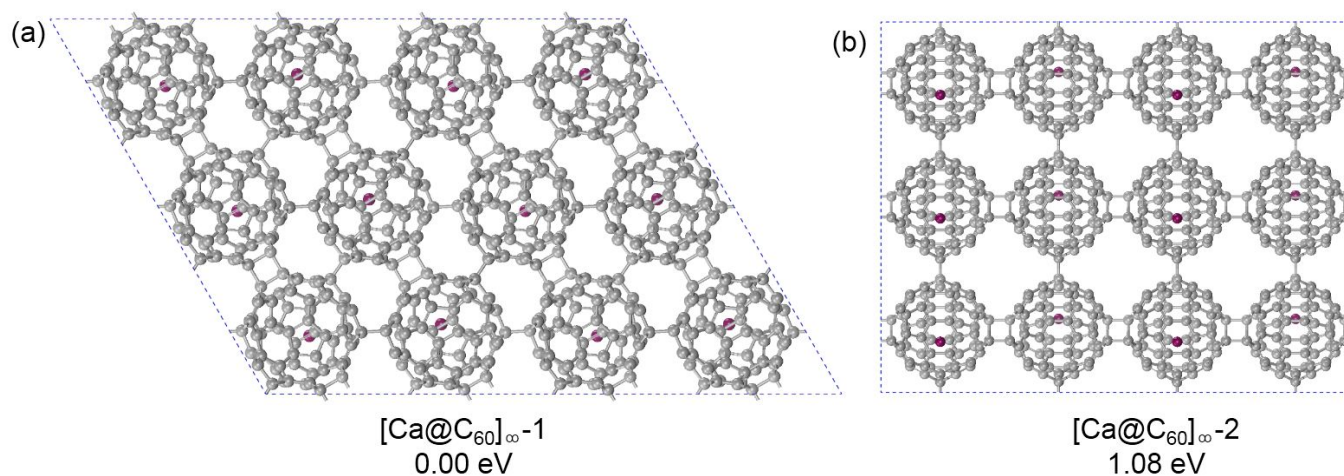


Figure 8. The optimized structures of $[\text{Ca@C}_{60}]_{\infty-1}$ and $[\text{Ca@C}_{60}]_{\infty-2}$. The calculated relative energies for a unit cell are shown.

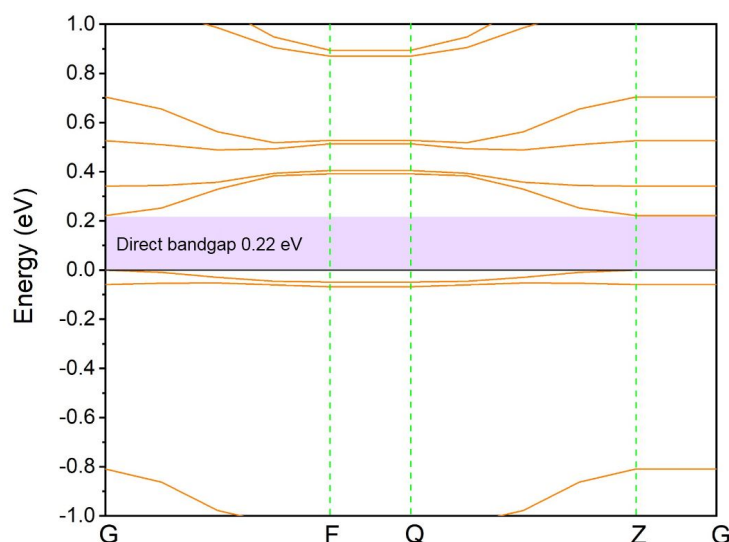


Figure 9. The calculated band structure of $[\text{Ca@C}_{60}]_{\infty-1}$.

3. Computational Details

DFT calculations were conducted on Ca@C_{60} and its oligomers and polymers. The oligomers included the dimer $[\text{Ca@C}_{60}]_2$, the trimer $[\text{Ca@C}_{60}]_3$ and the tetramer $[\text{Ca@C}_{60}]_4$. The polymers were referred to as $[\text{Ca@C}_{60}]_{\infty}$. Gaussian16 version A03 [37] was used for the calculations on the oligomers, with the PBE0 functional employed [38]. To account for the significant van der Waals interaction between the fullerene cages, the dispersion correction D3(BJ) was applied [39]. The geometric optimization utilized the def2SVP basis set for the carbon and calcium atoms [40], while the def2-TZVP basis set was used for single-point energy calculations [41]. The counterpoise method of Boys and Bernardi was employed to correct the basis set superposition error (BSSE) [42]. The interaction between Ca@C_{60} monomers was investigated using the MULTIWFN program [43], specifically the analysis of independent gradient model based on Hirshfeld partition (IGMH) [44,45]. The visualization of the calculation results was achieved using the Visual Molecular Dynamics (VMD, version 1.9.3) software [46].

We utilized the Dmol3 package [47,48] to perform calculations on the polymers $[\text{Ca@C}_{60}]_{\infty}$ within periodic models. The generalized gradient approximation (GGA) with the Perdew-Burke-Ernzerhof (PBE) functional [49] was applied to simulate the electron exchange correlation interaction. Electron-ion interactions were described using the DFT Semi-core Pseudopotentials (DSPP) [50]. The wave function is expanded by Double Numerical plus polarization (DNP) basis set, and the Brillouin zone is used by $2 \times 4 \times 1$ K-point grid for $[\text{Ca@C}_{60}]_{\infty}-1$, $4 \times 2 \times 1$ for $[\text{Ca@C}_{60}]_{\infty}-2$. The van der Waals interaction was described using the Tkatchenko-Scheffler method [51]. In order to prevent interlayer interaction between the same research objects, a 15 Å vacuum layer was applied.

4. Conclusions

We conducted a comprehensive investigation into the stability and electronic properties of oligomers and polymers of Ca@C_{60} through DFT calculations. In the most stable Ca@C_{60} dimer, the fullerene cages are connected through a four-atom ring, with each fullerene cage utilizing a (5,6) bond to form the four-atom ring. The trimer of Ca@C_{60} exhibits a most stable isomer with a triangular structure. For Ca@C_{60} tetramers, two thermodynamically stable isomers exist—one with a rectangular shape and the other with a rhombus shape. Our findings indicate a decreasing HOMO-LUMO gap as the number of Ca@C_{60} units increases to three and four in the oligomers. Furthermore, our study reveals that the oligomer formation is an exothermic process, with van der Waals interactions between fullerene cages playing a crucial role. In the case of the two-dimensional polymer of Ca@C_{60} , we observe structural similarities with graphullerene. This polymer functions as a semiconductor, featuring a direct bandgap of 0.22 eV. Given the solubility of the Ca@C_{60} monomer in aniline, future experimental studies on the polymerization of Ca@C_{60} are deemed feasible.

Author Contributions: Conceptualization, Z.W.; methodology, Y.W. and Z.Z.; software, Y.W. and Z.Z.; validation, Y.W. and Z.Z.; formal analysis, Y.W. and Z.Z.; investigation, Y.W. and Z.Z.; resources, Z.W.; data curation, Z.Z. and Z.W.; writing—original draft preparation, Z.W.; writing—review and editing, Z.W.; visualization, Y.W.; supervision, Z.W.; project administration, Z.W.; funding acquisition, Z.W. All authors have read and agreed to the published version of the manuscript.

Funding: This work was supported by the Beijing Municipal Natural Science Foundation (grant no. 2212030) and the National Natural Science Foundation of China (grant no. 22175199).

Institutional Review Board Statement: Not applicable.

Informed Consent Statement: Not applicable.

Data Availability Statement: The data presented in this study are available in this article.

Acknowledgments: We are grateful for the support of the Public Computing Cloud at Renmin University of China.

Conflicts of Interest: The authors declare no conflict of interest.

References

1. Lindle, J.; Pong, R.; Bartoli, F.; Kafafi, Z. Nonlinear optical properties of the fullerenes C_{60} and C_{70} at 1.064 μm . *Phys. Rev. B* **1993**, *48*, 9447. [[CrossRef](#)] [[PubMed](#)]
2. Sun, Y.P.; Lawson, G.E.; Riggs, J.E.; Ma, B.; Wang, N.; Moton, D.K. Photophysical and nonlinear optical properties of [60] fullerene derivatives. *J. Phys. Chem. A* **1998**, *102*, 5520–5528. [[CrossRef](#)]
3. Makarova, T. Electrical and optical properties of pristine and polymerized fullerenes. *Semiconductors* **2001**, *35*, 243–278. [[CrossRef](#)]
4. Sachdeva, S.; Singh, D.; Tripathi, S. Optical and electrical properties of fullerene C_{70} for solar cell applications. *Opt. Mater.* **2020**, *101*, 109717. [[CrossRef](#)]
5. Guo, K.; Li, N.; Bao, L.; Lu, X. Fullerenes and derivatives as electrocatalysts: Promises and challenges. *Green Energy Environ.* **2022**, *9*, 7–27. [[CrossRef](#)]
6. Huang, C.; Yang, Y.; Li, M.; Qi, X.; Pan, C.; Guo, K.; Bao, L.; Lu, X. Ultrahigh Capacity from Complexation-Enabled Aluminum-Ion Batteries with C_{70} as the Cathode. *Adv. Mater.* **2023**, 2306244. [[CrossRef](#)]
7. Li, C.Z.; Yip, H.L.; Jen, A.K.Y. Functional fullerenes for organic photovoltaics. *J. Mater. Chem.* **2012**, *22*, 4161–4177. [[CrossRef](#)]

8. Collavini, S.; Delgado, J.L. Fullerenes: The stars of photovoltaics. *Sustain. Energy Fuels* **2018**, *2*, 2480–2493. [[CrossRef](#)]
9. Castro, E.; Garcia, A.H.; Zavala, G.; Echegoyen, L. Fullerenes in biology and medicine. *J. Mater. Chem. B* **2017**, *5*, 6523–6535. [[CrossRef](#)]
10. Su, S.; Zhen, M.; Zhou, C.; Cao, X.; Sun, Z.; Xu, Y.; Li, L.; Jia, W.; Wu, Z.; Wang, C. Efficiently Inhibiting Systemic Inflammatory Cascades by Fullerenes for Retarding HFD-Fueled Atherosclerosis. *Adv. Healthc. Mater.* **2023**, *12*, 2202161. [[CrossRef](#)]
11. Burger, B.; Winter, J.; Kuzmany, H. Dimer and cluster formation in C₆₀ photoreaction. *Z. Phys. B Condens. Matter* **1996**, *101*, 227–233. [[CrossRef](#)]
12. Blank, V.D.; Buga, S.G.; Dubitsky, G.A.; Serebryanaya, N.R.; Popov, M.Y.; Sundqvist, B. High-pressure polymerized phases of C₆₀. *Carbon* **1998**, *36*, 319–343. [[CrossRef](#)]
13. Okada, S.; Saito, S. Electronic structure and energetics of pressure-induced two-dimensional C₆₀ polymers. *Phys. Rev. B* **1999**, *59*, 1930. [[CrossRef](#)]
14. Xu, C.H.; Scuseria, G.E. Theoretical predictions for a two-dimensional rhombohedral phase of solid C₆₀. *Phys. Rev. Lett.* **1995**, *74*, 274. [[CrossRef](#)] [[PubMed](#)]
15. Rao, A.; Eklund, P.; Venkateswaran, U.; Tucker, J.; Duncan, M.; Bendele, G.; Stephens, P.; Hodeau, J.L.; Marques, L.; Nunez-Regueiro, M.; et al. Properties of C₆₀ polymerized under high pressure and temperature. *Appl. Phys. A* **1997**, *64*, 231–2239. [[CrossRef](#)]
16. Giacalone, F.; Martin, N. Fullerene polymers: Synthesis and properties. *Chem. Rev.* **2006**, *106*, 5136–5190. [[CrossRef](#)]
17. Blank, V.; Buga, S.; Serebryanaya, N.; Denisov, V.; Dubitsky, G.; Ivlev, A.; Mavrin, B.; Popov, M.Y. Ultrahard and superhard carbon phases produced from C₆₀ by heating at high pressure: Structural and Raman studies. *Phys. Lett. A* **1995**, *205*, 208–216. [[CrossRef](#)]
18. Sabirov, D.S. Polarizability of C₆₀ fullerene dimer and oligomers: The unexpected enhancement and its use for rational design of fullerene-based nanostructures with adjustable properties. *RSC Adv.* **2013**, *3*, 19430–19439. [[CrossRef](#)]
19. Sabirov, D.S.; Ori, O.; Tukhbatullina, A.A.; Shepelevich, I.S. Covalently bonded fullerene nano-aggregates (C₆₀)_n: Digitalizing their energy–topology–symmetry. *Symmetry* **2021**, *13*, 1899. [[CrossRef](#)]
20. Hou, L.; Cui, X.; Guan, B.; Wang, S.; Li, R.; Liu, Y.; Zhu, D.; Zheng, J. Synthesis of a monolayer fullerene network. *Nature* **2022**, *606*, 507–510. [[CrossRef](#)]
21. Meirzadeh, E.; Evans, A.M.; Rezaee, M.; Milich, M.; Dionne, C.J.; Darlington, T.P.; Bao, S.T.; Bartholomew, A.K.; Handa, T.; Rizzo, D.J.; et al. A few-layer covalent network of fullerenes. *Nature* **2023**, *613*, 71–76. [[CrossRef](#)]
22. Argaman, U.; Makov, G. Structure and properties of graphullerene: A semiconducting two-dimensional C₆₀ crystal. *Npj Comput. Mater.* **2023**, *9*, 211. [[CrossRef](#)]
23. Shinohara, H. Endohedral metallofullerenes. *Rep. Prog. Phys.* **2000**, *63*, 843. [[CrossRef](#)]
24. Chaur, M.N.; Melin, F.; Ortiz, A.L.; Echegoyen, L. Chemical, electrochemical, and structural properties of endohedral metallofullerenes. *Angew. Chem. Int. Ed.* **2009**, *48*, 7514–7538. [[CrossRef](#)] [[PubMed](#)]
25. Cong, H.; Yu, B.; Akasaka, T.; Lu, X. Endohedral metallofullerenes: An unconventional core–shell coordination union. *Coord. Chem. Rev.* **2013**, *257*, 2880–2898. [[CrossRef](#)]
26. Popov, A.A.; Yang, S.; Dunsch, L. Endohedral fullerenes. *Chem. Rev.* **2013**, *113*, 5989–6113. [[CrossRef](#)] [[PubMed](#)]
27. Wang, T.; Wang, C. Endohedral Metallofullerenes Based on Spherical I_h-C₈₀ Cage: Molecular Structures and Paramagnetic Properties. *Acc. Chem. Res.* **2014**, *47*, 450–458. [[CrossRef](#)] [[PubMed](#)]
28. Yang, S.; Wei, T.; Jin, F. When metal clusters meet carbon cages: Endohedral clusterfullerenes. *Chem. Soc. Rev.* **2017**, *46*, 5005–5058. [[CrossRef](#)] [[PubMed](#)]
29. Jin, P.; Li, Y.; Magagula, S.; Chen, Z. Exohedral functionalization of endohedral metallofullerenes: Interplay between inside and outside. *Coord. Chem. Rev.* **2019**, *388*, 406–439. [[CrossRef](#)]
30. Shen, W.; Hu, S.; Lu, X. Endohedral metallofullerenes: New structures and unseen phenomena. *Chem.-Eur. J.* **2020**, *26*, 5748–5757. [[CrossRef](#)]
31. Li, M.; Zhao, R.; Dang, J.; Zhao, X. Theoretical study on the stabilities, electronic structures, and reaction and formation mechanisms of fullerenes and endohedral metallofullerenes. *Coord. Chem. Rev.* **2022**, *471*, 214762. [[CrossRef](#)]
32. Shen, W.; Bao, L.; Lu, X. Endohedral Metallofullerenes: An Ideal Platform of Sub-Nano Chemistry. *Chin. J. Chem.* **2022**, *40*, 275–284. [[CrossRef](#)]
33. Hu, Z.; Wang, Y.; Ullah, A.; Gutiérrez-Finol, G.M.; Bedoya-Pinto, A.; Gargiani, P.; Shi, D.; Yang, S.; Shi, Z.; Gaita-Ariño, A.; et al. High-temperature magnetic blocking in a monometallic dysprosium azafullerene single-molecule magnet. *Chem* **2023**, *9*, 3613–3622. [[CrossRef](#)]
34. Kubozono, Y.; Noto, T.; Ohta, T.; Maeda, H.; Kashino, S.; Emura, S.; Ukita, S.; Sogabe, T. Extractions of Ca@C₆₀ and Sr@C₆₀ with aniline. *Chem. Lett.* **1996**, *25*, 453–454. [[CrossRef](#)]
35. Wu, Y.; Jiang, Y.; Deng, J.; Wang, Z. Capturing unconventional metallofullerene M@C₆₀ through activation of the unreactive [5,6] bond toward Diels–Alder reaction. *Phys. Chem. Chem. Phys.* **2020**, *22*, 24249–24256. [[CrossRef](#)] [[PubMed](#)]
36. Ueno, H.; Aoyagi, S.; Yamazaki, Y.; Ohkubo, K.; Ikuma, N.; Okada, H.; Kato, T.; Matsuo, Y.; Fukuzumi, S.; Kokubo, K. Electrochemical reduction of cationic Li⁺@C₆₀ to neutral Li⁰@C₆₀⁻: isolation and characterisation of endohedral [60]fulleride. *Chem. Sci.* **2016**, *7*, 5770–5774. [[CrossRef](#)] [[PubMed](#)]
37. Frisch, M.J.; Trucks, G.W.; Schlegel, H.B.; Scuseria, G.E.; Robb, M.A.; Cheeseman, J.R.; Scalmani, G.; Barone, V.; Petersson, G.A.; Nakatsuji, H.; et al. *Gaussian 16*; Revision A.03; Gaussian Inc.: Wallingford, CT, USA, 2016.

38. Adamo, C.; Barone, V. Toward reliable density functional methods without adjustable parameters: The PBE0 model. *J. Chem. Phys.* **1999**, *110*, 6158–6170. [[CrossRef](#)]
39. Grimme, S.; Ehrlich, S.; Goerigk, L. Effect of the damping function in dispersion corrected density functional theory. *J. Comput. Chem.* **2011**, *32*, 1456–1465. [[CrossRef](#)]
40. Weigend, F.; Ahlrichs, R. Balanced basis sets of split valence, triple zeta valence and quadruple zeta valence quality for H to Rn: Design and assessment of accuracy. *Phys. Chem. Chem. Phys.* **2005**, *7*, 3297–3305. [[CrossRef](#)]
41. Schäfer, A.; Huber, C.; Ahlrichs, R. Fully Optimized Contracted Gaussian Basis Sets of Triple Zeta Valence Quality for Atoms Li to Kr. *J. Chem. Phys.* **1994**, *100*, 5829–5835. [[CrossRef](#)]
42. Boys, S.F.; Bernardi, F. The calculation of small molecular interactions by the differences of separate total energies. Some procedures with reduced errors. *Mol. Phys.* **1970**, *19*, 553–566. [[CrossRef](#)]
43. Lu, T.; Chen, F. Multiwfn: A multifunctional wavefunction analyzer. *J. Comput. Chem.* **2012**, *33*, 580–592. [[CrossRef](#)]
44. Lefebvre, C.; Rubez, G.; Khartabil, H.; Boisson, J.C.; Contreras-García, J.; Hénon, E. Accurately extracting the signature of intermolecular interactions present in the NCI plot of the reduced density gradient versus electron density. *Phys. Chem. Chem. Phys.* **2017**, *19*, 17928–17936. [[CrossRef](#)] [[PubMed](#)]
45. Lu, T.; Chen, Q. Independent gradient model based on Hirshfeld partition: A new method for visual study of interactions in chemical systems. *J. Comput. Chem.* **2022**, *43*, 539–555. [[CrossRef](#)] [[PubMed](#)]
46. Humphrey, W.; Dalke, A.; Schulten, K. VMD: Visual Molecular Dynamics. *J. Mol. Graph.* **1996**, *14*, 33–38. [[CrossRef](#)]
47. Delley, B. An all-electron numerical method for solving the local density functional for polyatomic molecules. *J. Chem. Phys.* **1990**, *92*, 508–517. [[CrossRef](#)]
48. Delley, B. From molecules to solids with the DMol 3 approach. *J. Chem. Phys.* **2000**, *113*, 7756–7764. [[CrossRef](#)]
49. Perdew, J.P.; Burke, K.; Ernzerhof, M. Generalized gradient approximation made simple. *Phys. Rev. Lett.* **1996**, *77*, 3865. [[CrossRef](#)]
50. Hamann, D.; Schlüter, M.; Chiang, C. Norm-conserving pseudopotentials. *Phys. Rev. Lett.* **1979**, *43*, 1494. [[CrossRef](#)]
51. Tkatchenko, A.; Scheffler, M. Accurate Molecular Van Der Waals Interactions from Ground-State Electron Density and Free-Atom Reference Data. *Phys. Rev. Lett.* **2009**, *102*, 073005. [[CrossRef](#)]

Disclaimer/Publisher’s Note: The statements, opinions and data contained in all publications are solely those of the individual author(s) and contributor(s) and not of MDPI and/or the editor(s). MDPI and/or the editor(s) disclaim responsibility for any injury to people or property resulting from any ideas, methods, instructions or products referred to in the content.